Inorganic Chemistry

Article

pubs.acs.org/IC

Structure and Magnetic Properties of the α-$NaFeO_2$-Type Honeycomb Compound $Na_3Ni_2BiO_6$

Elizabeth M. Seibel,*[,†] J. H. Roudebush,[†] Hui Wu,[‡,§] Qingzhen Huang,[‡] Mazhar N. Ali,[†] Huiwen Ji,[†] and R. J. Cava[†]

[†]Department of Chemistry, Princeton University, Princeton, New Jersey 08544, United States

[‡]NIST Center for Neutron Research, Gaithersburg, Maryland 20899-6102, United States

[§]Department of Materials Science and Engineering, University of Maryland, College Park, Maryland 20742-2115, United States

Supporting Information

ABSTRACT: We present the structure and magnetic properties of $Na_3Ni_2BiO_6$, which is an ordered variant of the α-$NaFeO_2$ structure type. This layered compound has a 2:1 ordering of $(Ni^{2+}/Bi^{5+})O_6$ octahedra within the *a*-*b* plane and sodium in octahedra between the layers. The structure is presented in the space group *C*2/*m*, determined through a combination of single crystal X-ray, powder neutron, and powder X-ray diffraction. Temperature dependent magnetic susceptibility measurements show $Na_3Ni_2BiO_6$ to display long-range antiferromagnetic ordering below 11 K, despite the dominance of ferromagnetic interactions above T_N as indicated by a positive Weiss constant. Heat capacity measurements and low-temperature neutron diffraction support the magnetic ordering and are consistent with a T_N of 10.4 K. A magnetic phase can be refined with (010) antiferromagnetic ordering along the *b*-axis in the honeycomb layer and moments aligned parallel to *c*. The compounds $Na_3Mg_2BiO_6$ and $Na_3Zn_2BiO_6$, synthesized as nonmagnetic analogues of $Na_3Ni_2BiO_6$, are briefly described.

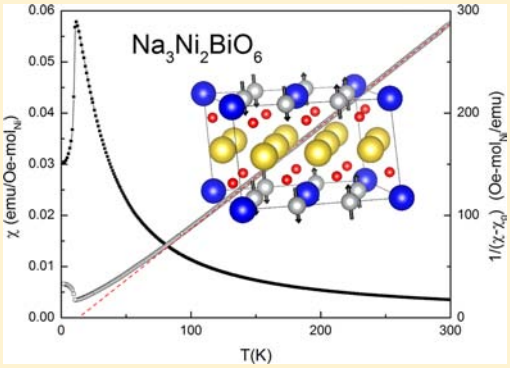

INTRODUCTION

Layered oxides of the Delafossite and α-$NaFeO_2$ structure types have been studied extensively for their wide range of properties.[1−4] The AMO_2 Delafossite and α-$NaFeO_2$ structures have MO_2 layers of edge sharing MO_6 octahedra. Typically Ag or Cu is linearly coordinated between the layers in the Delafossites, and an alkali is octahedrally coordinated between the layers in the $NaFeO_2$-type materials. Substitution of 1/3 of the *M*-site leads to $AM_{2/3}M'_{1/3}O_2$, where *M* and *M*′ can be in either the same or different oxidation states. When *M* and *M*′ adopt 2^+ and 5^+ oxidation states, respectively, the metals are frequently found to order within the plane in a 2:1 *M*:*M*′ fashion, such that the formula is written $Na_3M_2M'O_6$. Most work has focused on $M' = Sb^{5+}$, as in $Na_3M_2SbO_6$ (*M* = Mg, Ni, Co, Cu, Zn).[5−7] Each $M'O_6$ octahedron is surrounded in the plane by 6 edge-shared MO_6 octahedra, generating a honeycomb geometry for the *M* atoms. Recently, compounds with *M*′ = Bi^{5+} have been reported, including $Li_3NiMBiO_6$ (*M* = Mg, Ni, Cu, Zn)[8] and $Li_3Zn_2BiO_6$.[9] These are the only Bi^{5+}-based honeycombs reported to date, motivating the current work.

The honeycomb lattices described here are based on a triangular lattice where two-thirds of the metal sites in the $M_2M'O_6$ layer are magnetic (i.e., $M = Ni^{2+}$), and one-third are nonmagnetic (i.e., $M' = Sb^{5+}/Bi^{5+}$). When *M* is a magnetic ion, the honeycomb geometry offers the possibility for magnetic frustration. Though the honeycomb lattice is not traditionally considered frustrated, magnetic ions on a hexagonal net often experience frustration of their ordering that arises from competing, comparable nearest neighbor (NN) and next-nearest neighbor (NNN) magnetic interactions, leading to complex magnetic structures and often a depression of the long-range ordering temperature.[10,11,2] This competition has been of recent interest in the Na_2IrO_3 honeycomb structure, for example, where frustration among the Ir^{4+} ions on the honeycomb manifests itself in a relatively large θ_{cw}/T_N ratio.[12] Several ordered antiferromagnetic (AFM) structures have been proposed for Na_2IrO_3, including "zigzag," "stripy," and "Néel."[2] Despite overall AFM ordering, competing ferromagnetic (FM) and AFM interactions within the honeycomb have also been suggested for $Na_3Co_2SbO_6$,[6] and magnetic structural refinements show both FM and AFM couplings in $Cu_3Ni_2SbO_6$ and $Cu_3Co_2SbO_6$.[13] We discuss here the synthesis, structure, and magnetic properties of $Na_3M_2BiO_6$ (*M* = Ni, Mg, Zn), with a focus on the Ni variant because of its magnetic properties, which reflect the presence of magnetic frustration in the system.

Received: August 20, 2013
Published: November 15, 2013

   dx.doi.org/10.1021/ic402131e | *Inorg. Chem.* 2013, 52, 13605−13611

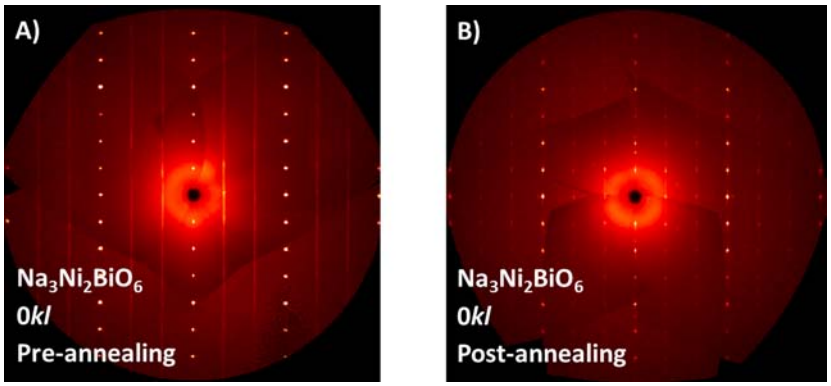

Figure 1. Single crystal diffraction of $Na_3Ni_2BiO_6$ along the 0*kl* projection. (A) Before annealing, significant streaking is seen along c^* consistent with coloring faults. (B) After annealing the cell can be indexed to the 1-layer $C2/m$ stacking type.

EXPERIMENTAL SECTION

Polycrystalline samples of $Na_3M_2BiO_6$ (M = Ni, Mg, Zn) were prepared by mixing dried, reagent-grade Na_2CO_3 and $NaBiO_3$ with NiO, $Mg(OH)_2$, or ZnO, respectively. Roughly 3% excess Na was added to compensate for possible volatilization, and the M:Bi ratio was stoichiometric. All reactions were carried out under flowing O_2. The nominal Ni mixture was ground, pressed into 1/2" diameter pellets, heated to 700 °C at 2 °C/min and held for 8 h in an alumina boat, then cooled to room temperature. This was followed by regrinding and reheating to 750 °C as a loose powder for an additional 12 h. The resulting compound was chestnut brown. The Mg sample was ground, heated as a loose powder in an alumina boat to 700 °C at 3 °C/min and held for 20 h, reground, and reheated to 725 °C for 2 h to yield a salmon-pink compound. The Zn compound was ground, heated as a loose powder to 700 °C at 3 °C/min and held for 40 h in an alumina boat, and then quenched to room temperature in air, followed by reheating at 700 °C for 8 h with a quench to room temperature to yield a peach-colored powder. The Zn compound could only be synthesized upon quenching; slow cooling yielded no quaternary product. The Mg and Zn samples were stored in a desiccator because of moisture sensitivity. All three materials showed some decomposition to Na_3BiO_4 + MO with additional heating.

Single crystals of $Na_3Ni_2BiO_6$ were successfully grown from a flux of 1:1 Na_2CO_3:Bi_2O_3. A 20 g mixture composed of 80% (by weight) flux and 20% polycrystalline $Na_3Ni_2BiO_6$ was ground and heated in an alumina crucible under flowing O_2 in a vertical tube furnace with a 25 °C vertical gradient across the 4 cm tall crucible. The flux was heated at 3 °C/min to 850 °C, held for 6 h, cooled to 750 °C at a rate of 0.02 °C/min, and then cooled to room temperature at a rate of 3 °C/min. The resulting crystals were thin (<0.2 mm), pseudohexagonal, transparent brown plates approximately 3−5 mm in diameter. Ordering along the c-axis was achieved by annealing crystals for 10 days at 500 °C under flowing O_2.

Polycrystalline samples were characterized by powder X-ray diffraction (pXRD) using a Bruker D8 FOCUS diffractometer with Cu Kα radiation and a diffracted beam monochromator. Single crystal X-ray diffraction (sXRD) was conducted on a Bruker APEX II detector with Mo Kα radiation (λ = 0.71703 Å) at 300 K. Neutron powder diffraction (NPD) patterns of the polycrystalline Ni sample were collected at 2.8 K, 25 K, and 300 K with wavelength 1.5403 Å on the BT-1 diffractometer at the NIST Center for Neutron Research. A Cu(311) monochromator with a 90° take off angle and in-pile collimation of 60 min of arc was used. Data were collected over the range of 3−160° 2θ with a step size of 0.05°. Powder diffraction patterns were refined using the FullProf suite,[14] and images generated with VESTA.[15]

Temperature-dependent magnetic susceptibility was measured on a Quantum Design Magnetic Property Measurement System (MPMS, model XL5). Zero field cooled (ZFC) magnetization data were taken from 2 to 300 K in an applied field of 1 T. All other measurements were taken on a Quantum Design Physical Property Measurement System (PPMS). Field dependent magnetization measurements were taken at 3, 6, 9, and 12 K with a sweep from −9 to 9 T. Heat capacity (HC) measurements were conducted from 2 to 250 K in zero applied field by mounting samples on a sapphire platform with Apiezon N grease for both $Na_3Ni_2BiO_6$ and $Na_3Mg_2BiO_6$. The latter nonmagnetic compound was employed to provide an estimate of the phonon contribution to the specific heat at low temperatures for $Na_3Ni_2BiO_6$. To estimate the magnetic contribution to the specific heat for $Na_3Ni_2BiO_6$, the HC data of the Ni and Mg samples were normalized to be equal at 140 K.

RESULTS AND DISCUSSION

Structure. There has been much discussion surrounding the layering scheme of α-$NaFeO_2$-type ordered honeycombs. Generally speaking, layered oxides of the form ABO_2 can have a range of intercalation site symmetries for the A cation, including octahedral, prismatic, trigonal, or linear (for Delafossites), based on the oxygen packing sequence.[1,16] In the α-$NaFeO_2$ structure type, the intercalation site is octahedral and all metal oxide octahedra have the same orientation, described by the notation "O3" (octahedrally coordinated sodium, 3 layers).[16] In honeycomb compounds, the 2:1 ordering of metal atoms in the a-b plane yields a unit cell larger by $\sqrt{3}a_0$ (where a_0 is basal plane cell parameter for α-$NaFeO_2$) that generates superlattice reflections not described by the $R\bar{3}m$ α-$NaFeO_2$ subcell.[17] Various models have been used to describe the superstructure, including examples in the centered monoclinic space groups $C2/m$ and $C2/c$, and the trigonal space group $P3_112$.[5−7] The distinction between $C2/m$ and $P3_112$ in a powder diffraction pattern can be challenging for these honeycomb structures because both can provide high figures of merit in fits, and the lattice parameters derived from $C2/m$ are often within error of trigonal metrics, as has been shown for Li_2MnO_3,[17] $Na_3Ni_2SbO_6$,[7] and $Na_3Co_2SbO_6$.[7] This frequently raises the question of whether the cell is truly hexagonal, or is monoclinic with pseudohexagonal metrics.[7,17] To compound this issue, irregular stacking of the metal oxide layers causes disorder and weakens the superlattice reflections. The disorder is observable in powder diffraction patterns as diffuse, asymmetric peaks that decrease in intensity toward higher angle. These are referred to as "stacking fault" or "Warren line shape" peaks.[18,19] Disorder in these honeycomb compounds occurs in the alignment of M and M′ atoms from layer to layer, and not in the orientation of octahedra (which would change the intercalation site symmetry). This alignment has been referred to as the layer "coloring" to distinguish it from a stacking fault in which the octahedral orientation or

dx.doi.org/10.1021/ic402131e | Inorg. Chem. 2013, 52, 13605−13611

Table 1. $Na_3Ni_2BiO_6$, Space Group $C2/m$ (no. 12); a = 5.3998(1) Å, b = 9.3518(2) Å, c = 5.67997(8) Å, β = 108.562(1)°, V = 271.91(1) Å^3, Z = 2[a]

atom	Wyckoff position	x	y	z	B_{iso}	occ.
Na(1)	2*d*	0	0.5	0.5	0.95(5)	1
Na(2)	4*h*	0.5	0.336(2)	0.5	0.95(5)	1
O(1)	8*j*	0.273(1)	0.3403(6)	0.7961(9)	0.52(3)	1
O(2)	4*i*	0.249(1)	0.5	0.212(1)	0.52(3)	1
Bi(1)	2*a*	0	0	0	0.44(2)	0.6382[b]
Ni(2)	2*a*	0	0	0	0.44(2)	0.3618[b]
Ni(1)	4*g*	0	0.66667[c]	0	0.44(2)	0.8191[b]
Bi(2)	4*g*	0	0.66667[c]	0	0.44(2)	0.1809[b]

[a] χ^2 = 1.08; wR_p = 7.31; R_p = 5.76; $R(F^2)$ = 6.39. [b] Fixed at the values determined from pXRD refinement (see text). [c] Fixed (see text). Fract(%): $Na_3Ni_2BiO_6$, 99.6(1); NiO, 0.4(1).

intercalation site symmetry changes.[13] One could think of $C2/m$, $C2/c$, and $P3_112$ as "O1", "O2", and "O3" packing, respectively.

$Na_3Ni_2BiO_6$ was refined in space group $C2/m$ based on a combination of sXRD, NPD, and lab pXRD. Refinements of lab pXRD were insufficient to distinguish between the three packing types as all gave acceptable fits, and both $C2/m$ and $P3_112$ yielded equivalent fits within error to a Rietveld refinement of the neutron data. Initially, single crystal data also seemed insufficient to distinguish the layer stacking because of significant streaking of the supercell reflections along the c^*-axis, indicating the presence of large numbers of coloring faults. Annealing these crystals at 500 °C, produced ordering along the c-axis that is fit exclusively to the 1-layer, $C2/m$ structural model (see Figure 1). Because some streaking of the superlattice reflections was still observed along c^*, atomic positions and occupancies were not refined from the single crystal X-ray data.

The lattice parameters obtained from the polycrystalline sample of composition $Na_3Ni_2BiO_6$ employed for the powder neutron diffraction study are in good agreement with those from the sXRD sample. The neutron diffraction data was then used to determine atomic positions while fixing all sites at full occupancy, assuming the $C2/m$ space group found from sXRD. In the honeycomb crystal structure, the Ni are in the Wyckoff 4*g* (0,*y*,0) sites while the Bi are in the Wyckoff 2*a* (0,0,0) sites (see Table 1). Refinement of the y parameter of the 4g (0,*y*,0) Ni-position led to a best fit for the y-value of 0.657. The validity of this was tested by fixing the Ni y-position to values of 0.645 to 0.675 in 0.005 increments and allowing all other parameters to refine freely. A broad shallow minimum in R_{wp} (7.32−7.33) existed in the range 0.657−0.675, which includes the y value of y = 0.66667 that is obtained for an ideal honeycomb lattice. Therefore, there is no statistical evidence for a distorted honeycomb. Given the virtually perfect hexagonal metrics of the in-plane monoclinic cell (i.e., $b/(a\sqrt{3})$ *and* $-(3c\cos\beta)/a$ are close to unity[7]) there is no evidence for the honeycomb to be anything other than ideal in shape. Therefore, the y coordinate was fixed at y = 0.66667 in the final model, and all other parameters were allowed to refine as detailed below.

The fraction of layer coloring was modeled by fixing the occupancies of Ni and Bi in the stoichiometric 2:1 ratio and then allowing for mixed atom occupancies on the Ni and Bi site.[13] This model is not meant to be representative of physical mixing of Ni and Bi within an individual layer; rather, the method provides a qualitative estimate of coloring faults because the faults are integrated into the average structure by the diffraction measurements. Because of the similarities in coherent scattering factors of Ni and Bi in neutron diffraction (10.3 and 8.5 fm, respectively),[20] no significant difference was observed in the fit to the data when stacking defects were introduced in the neutron pattern refinements. In contrast, because of the very large differences in X-ray scattering factors for Ni and Bi (Z = 28 and 83, respectively) XRD is more sensitive to this issue. When atomic positions were taken from neutron data and fixed in the pXRD refinement and occupancies allowed to refine as described above, the fit improved dramatically (χ^2 of ∼13 to ∼5) with ∼18% layer coloring. Sodium occupancies were found to be within experimental error of full occupancy and were then fixed. These occupancy values were then fixed in the neutron refinement, and all other parameters were allowed to freely refine to reach the final values presented in Table 1. The final neutron refinement yielded χ^2 = 1.08, and pXRD gave χ^2 = 5.24. An impurity phase (<0.5%) of NiO was present and accommodated in the refinement. Final refinements are shown in Figure 2, where asterisks mark superlattice reflections indicative of honeycomb ordering. The structure of $Na_3Ni_2BiO_6$ is shown in Figure 3, and atomic positions are given in Table 1. Selected bond distances are shown in Table 2. The Ni−Ni distance was found to be 3.117 Å (with fixed Ni position) and Ni−O bond lengths in the range 2.139(5)−2.158(3) Å. Bi−O bond lengths of 2.042(5) and 2.079(6) Å

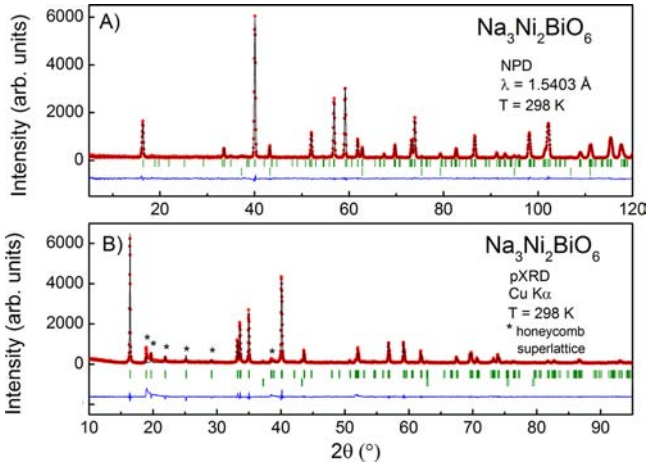

Figure 2. (A) NPD and (B) pXRD refinements of $Na_3Ni_2BiO_6$ taken at room temperature. Observed (red), calculated (black), and difference (blue) plots are shown, and Bragg reflections are indicated by green tick marks. The lower set of Bragg reflections belong to an NiO impurity phase.

dx.doi.org/10.1021/ic402131e | *Inorg. Chem.* 2013, 52, 13605−13611

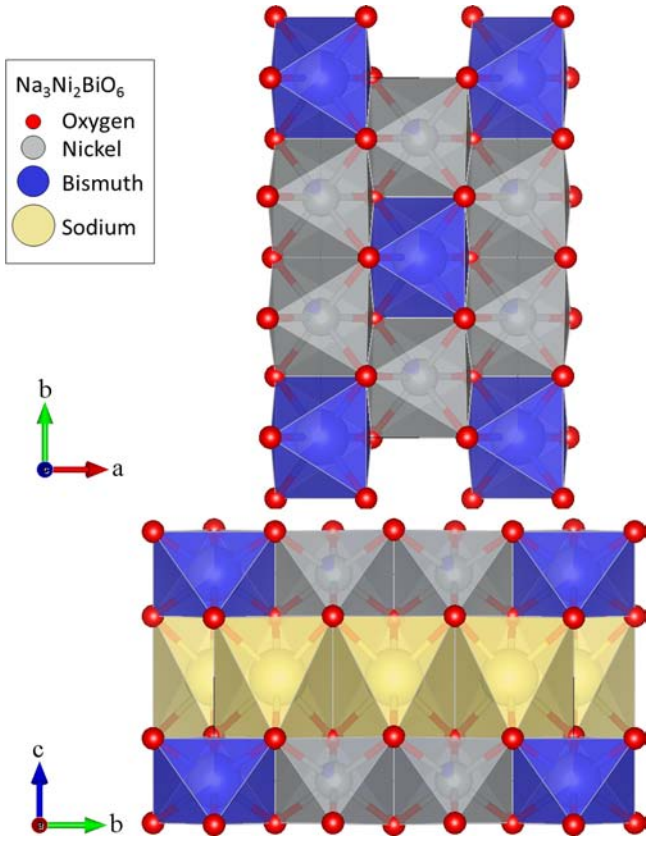

Figure 3. Structure of $Na_3Ni_2BiO_6$. Sodium is shown in yellow, oxygen in red, bismuth in blue, and nickel in gray. (A) The Ni/Bi honeycomb layer of edge-shared octahedra. (B) Projection perpendicular to the honeycomb layers. Sodium is also in octahedral coordination between the metal oxide layers.

Table 2. Selected $Na_3Ni_2BiO_6$ Bond Distances (Å) and Bond Angles (deg)

Ni(1)−O(1)×2	2.146(6)
Ni(1)−O(2)×2	2.158(3)
Ni(1)−O(1)×2	2.139(5)
Bi(1)−O(1)×4	2.042(5)
Bi(1)−O(2)×2	2.079(6)
Na(1)−O(1)×4	2.378(5)
Na(1)−O(2)×2	2.426(6)
Na(2)−O(1)×2	2.376(6)
Na(2)−O(1)×2	2.478(1)
Na(2)−O(2)×2	2.335(1)
Ni(1)−Ni(1)	3.117
Ni(1)−O(1)−Ni(1)	93.3(1)
Ni(1)−O(2)−Ni(1)	92.5(2)

indicate regular octahedra. The magnetization data (discussed below) is consistent with Ni^{2+}.

Profile fits of the isostructural compounds $Na_3Mg_2BiO_6$ and $Na_3Zn_2BiO_6$ are shown in Figure 4 and lattice parameters presented in Table 3. The pXRD data shows that these are 2:1 ordered honeycombs whose superlattice reflections are well-described by the $C2/m$ model, as indicated by asterisks in Figure 4. The samples contain small impurity phases of MgO and ZnO, respectively. These honeycombs follow the general trend of increasing a and b lattice parameters and cell volume in the order Ni < Mg < Zn, consistent with expected ionic radii (0.69 Å, 0.72 Å, and 0.74 Å, respectively)[21] though the c-axis parameter increases as Ni < Zn < Mg. This trend is the same as that reported for their sodium antimonate analogues.[7,22]

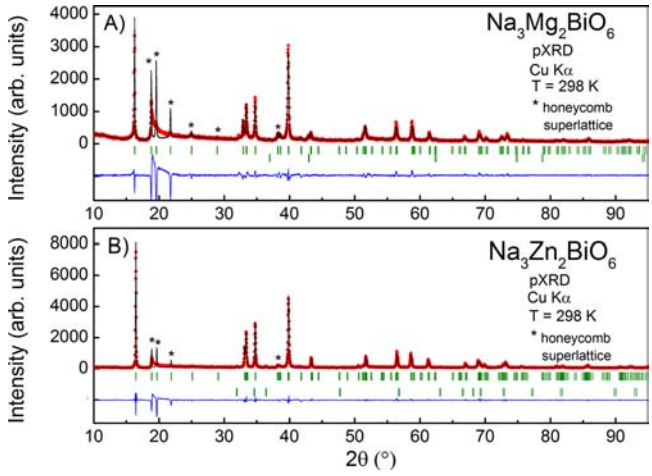

Figure 4. Profile fits of $Na_3Mg_2BiO_6$ (A) and $Na_3Zn_2BiO_6$ (B) in $C2/m$. Asterisks indicate Bragg reflections that are the result of 2:1 honeycomb ordering, as opposed to a disordered structure which would lack these reflections. Observed (red), calculated (black), and difference (blue) plots are shown, and Bragg reflections are indicated by green tick marks. The lower set of Bragg reflections belong to MgO and ZnO impurity phases, respectively.

Table 3. $Na_3M_2BiO_6$ (M = Ni, Mg, Zn) Lattice Parameters in $C2/m$

	$Na_3Ni_2BiO_6$[a]	$Na_3Mg_2BiO_6$[b]	$Na_3Zn_2BiO_6$[b]
a (Å)	5.3998(1)	5.4283(2)	5.4601(1)
b (Å)	9.3518(2)	9.4090(2)	9.4606(1)
c (Å)	5.67997(8)	5.7285(1)	5.71925(1)
β (deg)	108.562(1)	108.484(4)	108.526(1)
V (Å^3)	271.91(1)	277.49(1)	280.12(1)

[a]Rietveld refinement from NPD. [b]Profile fit from laboratory pXRD.

Magnetism. The temperature-dependent magnetization data for polycrystalline $Na_3Ni_2BiO_6$ is shown in Figure 5; a sharp decrease in the magnetic susceptibility, characteristic of AFM ordering, is clearly visible near 11 K (main panel). We take T_N to be 10.4 K based on a sharp magnetic ordering transition observed in HC measurements (discussed below). Curie−Weiss analysis ($\chi = C/(T - \theta)$ with a small correction ($\chi_0 = 4 \times 10^{-5}$) was used to fit the paramagnetic portion of the χ vs T data between 300 and 150 K. This yielded an effective moment of 2.8(1) μ_B/Ni^{2+}, consistent with the theoretical value assuming a spin-only contribution to the magnetic moment. Despite the long-range AFM ordering in $Na_3Ni_2BiO_6$, the positive Weiss temperature (θ_{CW}) of 13.3(1) K indicates dominantly FM interactions at high temperature. A positive Weiss temperature and AFM transition are characteristic of a frustrated system that arises from competition between nearest neighbor and higher order neighbor magnetic interactions.

The magnetic susceptibility data is similar to that seen in other Ni^{2+} honeycombs: all exhibit overall AFM ordering but a positive Weiss temperature. T_N of $Na_3Ni_2BiO_6$ is 10.4 K with θ_{CW} of 13.3(1) K, T_N of $Na_3Ni_2SbO_6$ is 18 K with θ_{CW} of 15 K,[22] T_N of $Li_3Ni_2BiO_6$ is 5.5 K with θ_{CW} of 20.1(6) K,[8] and T_N

dx.doi.org/10.1021/ic402131e | Inorg. Chem. 2013, 52, 13605−13611

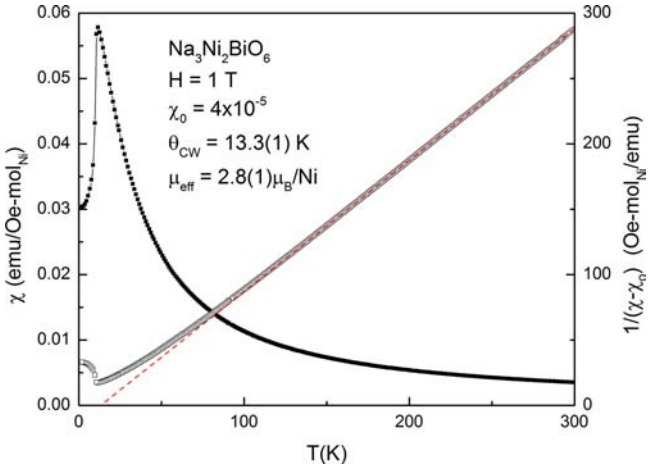

Figure 5. Susceptibility (χ) and inverse susceptibility ($1/(\chi - \chi_0)$) versus temperature in a 1 T field. An AFM ordering transition appears around 11 K, though the Curie fit (red, dashed line) from 150 K to room temperature yields a positive Weiss temperature of 13.3(1) K.

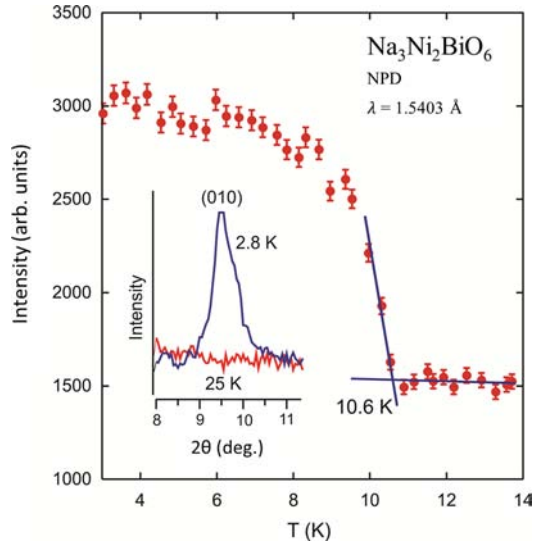

Figure 6. (010) Magnetic reflection observed in the 2.8 K neutron diffraction experiments. The figure shows the onset of the peak at 10.6 K, consistent with the ordering temperatures seen in the temperature-dependent magnetization and HC data. The inset shows the appearance of the peak at approximately 9.5° 2θ.

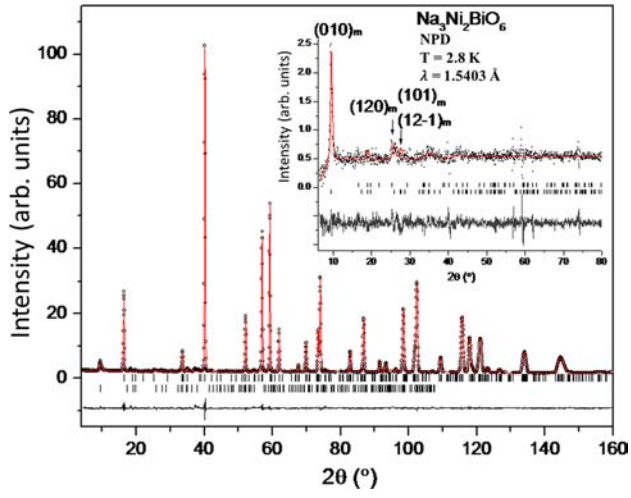

Figure 7. Experimental (circles), calculated (line), and difference (line below observed and calculated patterns) NPD profiles for $Na_3Ni_2BiO_6$ collected at 2.8 K ($C2/m$). Vertical bars indicate the calculated positions of Bragg peaks from the nuclear phase (top) and from the magnetic phase (bottom). Inset: Experimental (circles), calculated (line), and difference (line below observed and calculated patterns) NPD profiles for $Na_3Ni_2BiO_6$ obtained by subtraction of the 25 K pattern from the 2.8 K pattern. The subtracted NPD profile indicates the presence of magnetic reflections below the transition temperature. Vertical bars indicate the calculated positions of Bragg peaks from the nuclear phase (top) and from the magnetic phase (bottom). The relatively largely scattered experimental points are due to the difference from the nuclear phase diffraction peaks at two different temperatures.

of $Li_3Ni_2SbO_6$ is 15 K with θ_{CW} of 8 K[23]. The Néel temperature generally decreases on going from M' = Sb to M' = Bi (with the same alkali).[22] However, the magnitude of the Weiss constant does not follow a clear trend. For example, θ_{CW} decreases from $Na_3Ni_2SbO_6$ to $Na_3Ni_2BiO_6$, but increases from $Li_3Ni_2SbO_6$ to $Li_3Ni_2BiO_6$. This suggests that although all order antiferromagnetically, the FM contribution is different for each compound, and the origin of this may be complex. Though a magnetic model of in-plane FM ordering and interplane AFM coupling has been suggested for $Li_3Ni_2SbO_6$ and $Na_3Ni_2SbO_6$ based on Goodenough–Kanamori rules,[23,22] it seemed possible that the magnetism in $Na_3Ni_2BiO_6$ is more complicated than this model. To determine the ground state magnetic structure, we carried out low-temperature neutron diffraction experiments.

Our low temperature neutron diffraction data for a sample in zero applied field, shown in Figure 6, indicates magnetic ordering as evidenced by a relatively intense (010) reflection that is not present at 25 K. A magnetic structure model with the P_Cm Shubnikov group (#23) can satisfactorily fit the extra reflections, with AFM ordering within the plane of Ni, similar to the "zigzag" magnetic model for Na_2IrO_3.[2] The fit on the 2.8 K NPD pattern is shown in Figure 7 (R_{wp} = 0.0381, R_p = 0.0288). Refinement on the difference between the NPD patterns above and below the magnetic transition temperature was also performed (inset). We note that the extraneous reflection at ~18° 2θ appears at both 25 and 2.8 K, and is therefore from an unknown impurity phase and is not a magnetic reflection. From the refined magnetic structure (Figure 8), Ni shows AFM ordering along the b direction, with moments aligned ferromagnetically along c. Ferromagnetic zigzag chains run parallel to a within the plane. The magnetic moments obtained from both refinements (low temperature, and difference between low and high temperature) were consistent with an ordered Ni moment of 2.21(2) μ_B aligned along the c-axis, that is, perpendicular to the plane of the honeycomb. The FM coupling between planes may be related to the stacking of Ni atoms from one honeycomb layer to the next. The (010) magnetic reflection is fairly diffuse and asymmetric with a tail toward high angle. This may indicate the presence of small AFM ordered domains, two-dimensional magnetic order, or could be the result of the structural stacking faults. Note that an unambiguous magnetic model cannot be determined from the present NPD data because of the limited number of magnetic reflections observed and their rather weak intensities. Further experimentation on single crystals may be of interest. Nevertheless, the current AFM structure model can be used to fit the 2.8 K NPD pattern reasonably well and is consistent with our magnetization results.

dx.doi.org/10.1021/ic402131e | Inorg. Chem. 2013, 52, 13605–13611

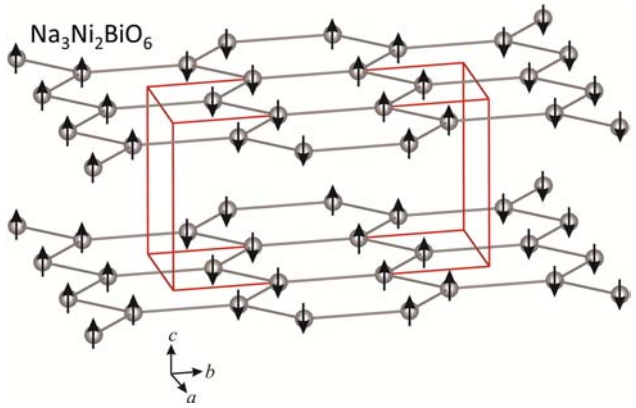

Figure 8. AFM structure model of $Na_3Ni_2BiO_6$ within Ni honeycomb lattice. Na, Bi, and O are omitted for clarity. Ni atoms exhibit AFM order along *b* direction with magnetic moments along *c* axis. AFM coupling exists within each Ni honeycomb plane and FM coupling between planes.

The characterization of the magnetic transition through the measurement of the HC was performed; the HC data are presented in Figure 9. An ordering transition is seen in the HC

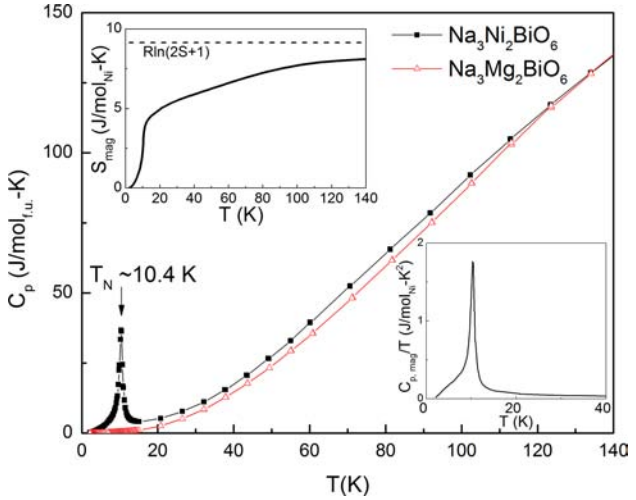

Figure 9. HC data for Ni and Mg and the resulting estimation of magnetic entropy (insets). Mg is shown as red, open triangles and Ni as black, filled squares. The magnetic entropy of Ni saturates around the value expected for a spin-only contribution (dashed line in upper-left inset). The lower-right inset shows the magnetic contribution to the HC ($C_{p,mag}$). T_N is indicated at 10.4 K in the main panel.

of $Na_3Ni_2BiO_6$, observed through the presence of the sharp peak in C_P at 10.4 K. This temperature is consistent with the ordering temperature seen in the temperature-dependent susceptibility and the appearance of the magnetic neutron diffraction peak, and we therefore take 10.4 K to be T_N. $Na_3Mg_2BiO_6$ was chosen as the nonmagnetic analogue for subtraction of the phonon contribution because its cell volume is close to that of the Ni phase. To estimate the phonon contribution for $Na_3Ni_2BiO_6$, the HCs of both compounds were normalized to be equal at 140 K. The HC of the Mg compound was then subtracted from that of the Ni compound to remove the phonon contribution and estimate the magnetic contribution to the HC. The magnetic entropy was estimated by integrating C_p/T dT. As shown in the inset of Figure 9, the magnetic entropy ultimately saturates at around 8.1 J/mol-K at 140 K, close to the value expected for Ni^{2+} (S = 1) with a spin-only contribution given by R ln(2S + 1). The magnetic entropy loss occurs in two regions on cooling, first over a broad range between 140 and 15 K, characteristic of 2D ordering within the plane, then a sharp loss in entropy at the 3D ordering transition near 11 K. This is characteristic of a low dimensional magnetic system with significant short-range magnetic ordering above the three-dimensional ordering temperature.

Field-dependent magnetization data collected at low temperatures for $Na_3Ni_2BiO_6$ is presented in Figure 10. No hysteresis

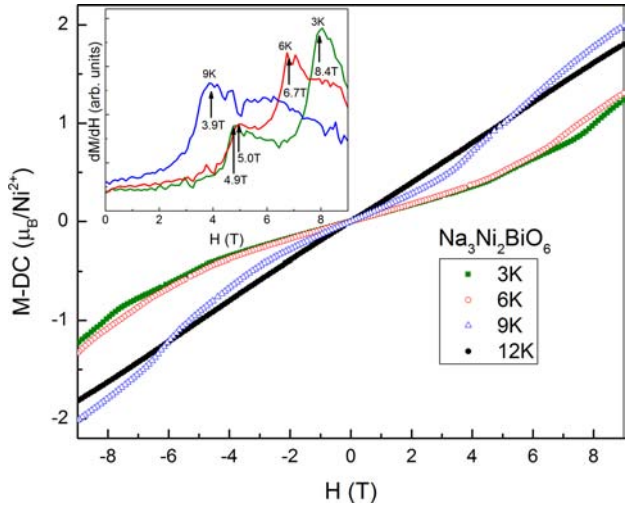

Figure 10. Field-dependent magnetization of $Na_3Ni_2BiO_6$. Data collected at 3 K shown as filled, green squares; 6 K as open, red circles; 9 K as open, blue triangles; and 12 K as filled, black circles. Upper-left inset, dM/dH vs H, suggests magnetic phase transitions at temperatures indicated by black arrows.

is observed, and the field-induced magnetization is linear up to applied fields of $\mu_0 H$ = 9 T above T_N. However, below T_N, distinct magnetic phases emerge. Two magnetic phases are evidenced by peaks in dM/dH vs H (inset) at 3 and 6 K. The first transition occurs at approximately the same field (5 T) at both temperatures, but the second transition is observed at 8 T at 3 K and 7 T at 6 K. At 9 K, closer to T_N, one transition is visible, beginning at 3.9 T, followed by a possible broad transition at higher applied field. The observed behavior is consistent with a frustrated system for which the small FM energies imposed by applied fields less than 9 T are enough to tip the magnetic ordering from one type to another.

CONCLUSIONS

The crystal structure of $Na_3Ni_2BiO_6$ was refined in space group $C2/m$ based on a combination of single crystal diffraction, neutron diffraction, and pXRD. This compound is an extension of the α-$NaFeO_2$ structure type with 2:1 ordering of metals on the M-site that generates a layered honeycomb. Despite the long-range AFM ordering transition seen in the temperature-dependent susceptibility measurements, the compound has a positive Weiss temperature indicative of dominant FM interactions above T_N. Magnetic data, HC, and neutron diffraction are all consistent with a T_N of ~11 K, though we assign T_N as 10.4 K based on the sharp ordering transition in the HC. We suggest a possible AFM structure where magnetic moments align parallel to the *c*-axis but are coupled antiferromagnetically along the *b*-axis within the honeycomb

dx.doi.org/10.1021/ic402131e | *Inorg. Chem.* 2013, 52, 13605−13611

layer, with FM zigzag chains running parallel to the *a*-axis within the layer. The neutron diffraction, specific heat, magnetic susceptibility, and field dependent magnetization measurements taken together suggest that further studies would be of interest to carefully characterize the magnetic phase diagram of $Na_3Ni_2BiO_6$. Research on an oxyhydrate of $Na_3Ni_2BiO_6$, as in the spin 1/2 honeycomb system $Na_{0.95}Ni_2SbO_6{\cdot}1.5H_2O$, is currently in progress.[24]

■ ASSOCIATED CONTENT

Ⓢ Supporting Information

Cystallographic data in CIF format. This material is available free of charge via the Internet at http://pubs.acs.org..

■ AUTHOR INFORMATION

Corresponding Author

*E-mail: eseibel@princeton.edu.

Notes

The authors declare no competing financial interest.

■ ACKNOWLEDGMENTS

This work was supported by the DOE through the Institute for Quantum Matter at Johns Hopkins University, Grant DE-FG02-08ER45644. The authors would like to thank Jason Krizan, Kristen Baroudi, and David Huse for helpful discussions.

■ REFERENCES

(1) Marquardt, M.; Ashmore, N.; Cann, D. *Thin Solid Films* **2006**, *496*, 146−156.
(2) Chaloupka, J.; Jackeli, G.; Khaliullin, G. *Phys. Rev. Lett.* **2013**, *110*, 097204.
(3) Takada, K.; Sakurai, H.; Takayama-Muromachi, E.; Izumi, F.; Dilanian, R. A.; Sasaki, T. *Nature* **2003**, *422*, 53−55.
(4) Goodenough, J. B.; Kim, Y. *Chem. Mater.* **2010**, *22*, 587−603.
(5) Smirnova, O. A.; Nalbandyan, V. B.; Petrenko, A. A.; Avdeev, M. *J. Solid State Chem.* **2005**, *178*, 1165−1170.
(6) Viciu, L.; Huang, Q.; Morosan, E.; Zandbergen, H. W.; Greenbaum, N. I.; McQueen, T.; Cava, R. J. *J. Solid State Chem.* **2007**, *180*, 1060−1067.
(7) Politaev, V. V.; Nalbandyan, V. B.; Petrenko, A. A.; Shukaev, I. L.; Volotchaev, V. A.; Medvedev, B. S. *J. Solid State Chem.* **2010**, *183*, 684−691.
(8) Berthelot, R.; Schmidt, W.; Muir, S.; Eilertsen, J.; Etienne, L.; Sleight, A. W.; Subramanian, M. A. *Inorg. Chem.* **2012**, *51*, 5377−5385.
(9) Greaves, C.; Katib, S. M. A. *Mater. Res. Bull.* **1990**, *25*, 1175−1182.
(10) Regnault, L.; Rossat-Mignod, J. Phase Transitions in Quasi Two-Dimensional Planar Magnets. In *Magnetic Properties of Layered Transition Metal Compounds*; Kluwer: Dordrecht, The Netherlands, 1989; pp 271−321.
(11) Smirnova, O.; Azuma, M.; Kumada, N.; Kusano, Y.; Matsuda, M.; Shimakawa, Y.; Takei, T. *J. Am. Chem. Soc.* **2009**, *131*, 8313−8317.
(12) Jin, H.; Kim, H.; Jeong, H.; Kim, C.; Yu, J. *arXiv:0907.0743v1*, **2009**.
(13) Roudebush, J. H.; Andersen, N. H.; Ramlau, R.; Garlea, V. O.; Toft-Petersen, R.; Norby, P.; Schneider, R.; Hay, J. N.; Cava, R. J. *Inorg. Chem.* **2013**, *52*, 6083−6095.
(14) Rodriguez-Carvajal, J. *Phys. B.* **1993**, *192*, 55−69.
(15) Momma, K.; Izumi, F. *J. Appl. Crystallogr.* **2008**, *41*, 653−658.
(16) Delmas, C.; Fouassier, C.; Hagenmuller, P. *Phys. B & C* **1980**, *99*, 81−85.
(17) Breger, J.; Jiang, M.; Dupre, N.; Meng, Y. S.; Shao-Horn, Y.; Ceder, G.; Grey, C. P. *J. Solid State Chem.* **2005**, *178*, 2575−2585.
(18) Todorova, V. L.; Leineweber, A.; Kienle, L.; Duppel, V.; Jansen, M. *J. Solid State Chem.* **2011**, *184*, 1112−1119.
(19) Warren, B. E. *Phys. Rev.* **1941**, *59*, 693−698.
(20) Sears, V. F. *Neutron News* **1992**, *3*, 26−37.
(21) Shannon, R. D.; Prewitt, C. T. *Acta Crystallogr, Sect. B: Struct. Crystallogr. Cryst. Chem.* **1969**, *25*, 925−946.
(22) Schmidt, W.; Berthelot, R.; Sleight, A. W.; Subramanian, M. A. *J. Solid State Chem.* **2013**, *201*, 178−185.
(23) Zvereva, E. A.; Evstigneeva, M. A.; Nalbandyan, V. B.; Savelieva, O. A.; Ibragimov, S. A.; Volkova, O. S.; Medvedeva, L. I.; Vasiliev, A. N.; Klingeler, R.; Buechner, B. *Dalton Trans.* **2012**, *41*, 572−580.
(24) Roudebush, J. H.; Cava, R. J. *J. Solid State Chem.* **2013**, *204*, 178−185.